Supporting Information for

"Peptidergic modulation of motor neuron output via CART signaling at C bouton synapses"

Panagiotis E. Eleftheriadis & Konstantinos Pothakos *et al.*

*Corresponding author. Email: lzagoraiou@bioacademy.gr

This PDF file includes:

- Supplementary Results
- SI Appendix – Materials and Methods
- Figs. S1 to S10
- Tables S1 to S4
- Supplementary References

Supplementary Results

Colocalisation of CART and ChAT in C bouton synapses (Fig. S3A), and in some motor neuron somata (Fig. S3B) was further supported by additional experiments in spinal cord sections from *Pitx2::Cre;Rosa.lsl.tdTomato* mice, where C bouton synapses were visualized with tdTomato. Using the IMARIS Image Analysis software (Oxford Instruments) on deconvolved confocal images, two different 3D surfaces were created that outline the volumes of interest (tdTomato: red surface, CART: green surface) revealing the partial or complete enclosure of the CART surfaces in the synapse (Fig. S3Ci-Ciii, Di-Diii, Fig. S4). Further observations of CART immunoreactivity patterns at C bouton synapses revealed a heterogenous distribution of CART within the presynaptic terminal. Synapses from spinal cords of *Pitx2::Cre;Rosa.lsl.tdTomato* mice and wild type mice (n=3 for each genotype, 400-700 synapses/mouse); labelled with anti-vesicular acetylcholine transporter (vAChT) and anti-CART antibodies were examined. Both approaches revealed four discrete distribution patterns of the CART neuropeptide in C bouton synapses (Fig. S3E-I). These included: i) "compact" synapses with an interior almost completely filled with the CART neuropeptide (Fig. S3E); ii) synapses with "puncta along the synapse" that had 3 or more CART+ puncta along the length of the synapse (Fig. S3F); iii) synapses with 1-3 puncta (Fig. S3G); and iv) also synapses with "peripheral puncta" that exhibited CART+ puncta at both ends of the synapse (Fig. S3H). Finally, we also observed cholinergic synapses that were devoid of the CART peptide (Fig. S3I). All CART distribution patterns were observed across postnatal development and through adulthood of mice (p10, p25, 8-9 weeks old, six months old, one year old; Table 1), suggesting that this diversity is a general feature of CART at C bouton synapses.

SI Appendix – Materials and Methods

Differential expression screen and *in situ* hybridization

The differential mRNA expression screen was performed as described in (1). Briefly upper lumbar (L1-L3) spinal cord segments from P8 mice were isolated and mounted in 2% agarose. The embedded segments were sectioned (Leica VT1000 S Vibrating blade microtome, 200-250µm) and each section was dissected. The intermediate zone was discarded. Dorsal and ventral parts were collected after white matter removal (Fig. 1A). RNA was isolated (n = 3 or 4 mice per sample) using the RNeasy Mini Kit (QIAGEN), and aRNA was synthesized with Ambion's MessageAmp aRNA Kit (Catalog # 1750) using Biotin 11-CTP and Biotin 16-UTP (Enzo). Affymetrix Gene chip Mouse Genome 430 2.0 Arrays were hybridized. Gene Traffic software was used for data analysis. The *in situ* hybridization experiments for the detection of CART and Pitx2 mRNA expression in spinal cord cross sections (Leica CM3050 S cryostat) were performed as described in (2)

Tissue preparation and immunohistochemistry

Spinal cords were isolated by anesthetizing animals with intraperitoneal injections (15µL/g body weight) of ketamine (10mg/mL) and xylazine (2 mg/mL) prior to performing transcardial perfusion with cold 4% paraformaldehyde (PFA) in PBS (the perfusion was omitted in P0 mice). Spinal cords were isolated and post-fixed in 4% PFA (2h), then washed in PBS (4 times) and cryoprotected in a 30% sucrose solution under slight rocking (4^{o}C) overnight. Spinal cords were further dissected (cervical, thoracic, upper lumbar and lower lumbar segments separation), and embedded in Tissue-Tek OCT medium. The immunohistochemistry experiments were performed in 15-20µm cryostat sections that were collected with positively charged or polylysine covered slides and stored at -80^{o}C after drying in RT. The sections were washed with PBS and were incubated with a 1% BSA- 0,1%Triton-X-100 in PBS solution containing the primary antibodies inside a humidified chamber at 4^{o}C overnight. Next the sections were incubated with fluorescently labeled secondary antibodies for 2h, were washed with PBS (4 times for 5 minutes) and covered in Vectashield mounting medium. Antibodies used: Rabbit anti CART (Phoenix Pharmaceuticals, G003-62), rabbit anti ChAT (Jessell lab, CU1574), rabbit anti vAChT (Jessell lab, CU1475), rabbit anti Pitx2 (Jessell lab, CU1533), rabbit anti M2 (Alomone labs, AB9452), guinea-pig anti vAChT (Fitzerald, 20R-VP002), goat anti vAChT (Millipore, ABN100), goat anti ChAT (Millipore, AB144P).

Mouse Lines

For all the experiments both male and female animals were utilized. No differences were observed in the anatomy experiments so data were pooled. In the behavioral experiments sex-dependent differences were observed and data were analyzed separately. The following mouse lines were used: *Pitx2::Cre* (3), *Rosa.stop.tdTomato* (4), *Dbx1::Cre* (5), *ChAT* $^{fl/fl}$ (6, 7), *CART*$^{KO/KO}$ (8). All genotypes mentioned in this manuscript were a result of elaborate selective breeding of the aforementioned mouse lines. Mice 4-6 months old were used for the behavioral experiments. The use of the specific *CART*$^{KO/KO}$ mouse line (8) allowed us to perform the motor performance test coherently as the weight gain caused by the complete knockout of the CART gene was detectable only after 40 weeks of age. Anatomy and behavioral experiments were performed in the animal facility of the Center for Clinical, Experimental Surgery and Translational Research of the Biomedical Research Foundation of the Academy of Athens. The facility is registered as "breeding" and "user" establishment by the Veterinary Service of the Prefecture of Athens according to the Presidential Decree 56/2013 in harmonization to the European Directive 63/2010 for the protection of animals used for scientific purposes. User establishment is also ISO 9001:2015 accredited. All animals of the facility were regularly screened using a health monitoring program, in accordance to the Federation of European Laboratory Animal Science Associations' recommendations.

Statistical analysis of anatomy data

A total of n=3, *Dbx1::Cre;ChAT*$^{fl/fl}$*;CART*$^{KO/KO}$ (experimental) and n=4 control mice were used for the synaptic counts. The vAChT+ terminals, postsynaptic M2 receptors and their close apposition were counted form single confocal images that translate to a physical section thickness of 1,208 μm (optical section), using Fiji (9). The normality of the distribution of counts within the experimental and control groups was assessed using the Shapiro-Wilk test and the non-parametric Mann-Whitney U test was used to compare group ranks (GraphPad Prism version 9.0.0 for Windows, GraphPad Software, San Diego, California USA, www.graphpad.com). The bar-charts representing the mean number of synapses per motor neuron section with the superimposed data points, representing data distribution, were also designed with GraphPad Prism 9.0.0. The median value is also presented as a red dot superimposed in each graph. Similarly, n=3, *Dbx1::Cre;ChAT*$^{fl/fl}$*;CART*$^{KO/KO}$ (experimental) and n = 3 control mice were used to evaluate the size of vAChT+ terminals and M2 postsynaptic clusters. In control animals 250 synapses were examined and tested against 228 synapses from experimental animals, using the Mann-Whitney U-test. The same procedure was followed for the 254 control and 225 experimental synapses evaluated for the size of M2 clusters. Data are presented as mean values (±SEM) and were combined as no sex-dependent differences where observed. Statistical significance was set at $a < 0.05$ for all measures.

Confocal Imaging and Image analysis using IMARIS (Oxford Instruments)

The 3-Dimensional stack images were captured using a 63x/1.4 NA oil immersion lens and a confocal laser scanning microscope (LeicaTC S SP5 II) in 1024x1024 pixel format. Single images, corresponding to physical thickness of 1,208 μm were used for anatomical analysis and the synapse counting procedures. All 63x images of motor neurons (presented in main text) are comprised of a collapsed z-stack image of 3 consecutive images in the z plane. The z-stack images were used for the reconstruction of the synapse with IMARIS. Using spinal cord sections of *Rosa.lsl.tdTomato* transgenic mice incubated with antibodies against dsRed and CART the colocalization of the CART peptide in C bouton synapses was visualized. First, confocal images were deconvolved using LAS AF (Leica Microsystems – Blind Deconvolution option) in order to reduce out of focus fluorescence and improve contrast allowing for the accurate reconstruction of < 1 μm structures. Using the surface rendering module of IMARIS, two different volumes were created (3D surfaces) based on the fluorescence intensity and size (red: C bouton synapse; green: CART peptide). The overlap of the surfaces and the

enclosure of the CART peptide surface (green) in the C bouton surface (red) was visualized by rendering the synapse exterior (red surface) transparent.

Tissue preparation for electrophysiology

Experiments were performed on male and female wild type C57 BlJ/6 mice from postnatal days 7-12 (n= 30). All procedures were approved by the Home Office and the University of St. Andrews Animal Care Committee. All animals were sacrificed by performing a cervical dislocation followed by rapid decapitation. Animals were eviscerated and pinned ventral side up in a dissecting chamber lined with silicone elastomer (Sylgard) filled with carbogenated (95% oxygen, 5% carbon dioxide), pre-chilled (1-4 degrees Celsius) dissecting artificial cerebrospinal fluid (aCSF; in mM: 25 NaCl, 188 sucrose, 1.9 KCl, 1.2 NaH2PO4, 10 MgSO4, 1 CaCl, 26 NaHCO3, 25 D-glucose, 1.5 kynurenic acid). Spinal cords were exposed by performing a ventral laminectomy, ventral roots cut and gently lifted from the spinal column. The lumbar section of the spinal cord was then secured with the ventral surface facing out to an agar block with surgical glue (Vetbond). The agar block was secured to the base of the slicing chamber with super glue. Slices from rostral (L1-L3) or caudal (L4-L6) segments were obtained on different days by placing the rostral or caudal segments facing up. The slicing chamber was filled with pre-chilled (1 - 4 degrees Celsius) carbogenated dissecting aCSF and 300 µm transverse slices made with a cutting speed of 100 µm/s on a Leica Vibratome (Leica, CT1200). Slices were transferred to a recovery chamber filled with carbogenated pre-warmed (35 degrees Celsius) recovery aCSF (in mM: 119 NaCl, 1.9 KCl, 1.2 NaH2PO4, 10 MgSO4, 1 CaCl, 26 NaHCO3, 20 glucose, 1.5 kynurenic acid, 3% dextran) for thirty minutes after completion of the last slice. Following recovery, slices were transferred to a chamber filled with carbogenated warm (35 degrees Celsius) recording aCSF (in mM: 127 NaCl, 3 KCl, 1.25 NaH2PO4, 1 MgCl, 2 CaCl2, 26 NaHCO3, 10 glucose) which was then allowed to equilibrate at room temperature (23-25 degrees Celsius) for at least one hour before experiments were initiated.

Whole cell patch clamp electrophysiology

Whole cell patch clamp recordings were obtained from motor neurons of the lateral motor column of in slice preparations of rostral and caudal lumbar segments. Slices were stabilized in a recording chamber with fine fibers secured to a platinum harp and visualized on an Olympus BX51WI microscope under a 40x objective with infrared illumination and differential interference (DIC) contrast. Whole cell recordings were obtained under DIC illumination with pipettes (L: 100 mm, OD: 1.5 mm, ID: 0.84 mm; World Precision Instruments) pulled on a Flaming Brown micropipette puller (Sutter instruments P97) to a resistance of 3-4 MOhms. Pipettes were back-filled with intracellular solution (in mM: 140 KMeSO4, 10 NaCl, 1 CaCl2, 10 HEPES, 1 EGTA, 3 Mg-ATP and 0.4 GTP-Na2; pH 7.2-7.3, adjusted with KOH), attached to an electrode holder and preamplifier (Molecular Devices CV-7B), which were positioned with a Patch Star micromanipulator (Scientifica, UK). Signals were amplified and filtered (6 kHz low pass Bessel filter) with a Multiclamp 700 B amplifier, acquired at 20 kHz using a Digidata 1440A digitizer with pClamp Version 10.7 software (Molecular Devices) and stored on a computer for offline analysis. Current clamp recordings were whole-cell capacitance compensated using Multiclamp Commander software.

Motor neurons were identified based on location in the ventrolateral region with somata greater than 20 µm. Intrinsic properties were only measured if cells had an initial resting membrane potential below -50 mV or if access resistance was less than 20 MΩ. All recordings were performed on cells in spinal cord slices that were naive to drug treatment with no more than one cell studied per slice. Cells were excluded from analysis if access resistance changed by more than 20% of the initial value or if action potential amplitude was less than 60 mV measured from threshold. Motor neuron intrinsic properties were studied by applying a bias current to maintain the membrane potential at -60mV. All values reported are not liquid junction potential corrected to facilitate comparisons with previously published data.

Identification of fast and slow motor neuron types

Fast and slow motor neurons were identified as by (10, 11) based on the onset latency at repetitive firing threshold using a 5 second square depolarizing current at rheobase. Using this approach, we were able to identify 2 repetitive firing profiles - a delayed repetitive firing with accelerating spike frequency characteristic of fast-type motor neurons and an immediate firing profile characteristic of slow type motor neurons (10–12).

Pharmacology

The cocaine and amphetamine regulated transcript peptide (CART acetate salt; 48 Amino Acid sequence: IPIYEKKYGQVPMCDAGEQCAVRKGARIGKLCDCPRGTSCNSFLLKCL; with triple disulfide bonds at Cys14 - Cys32, Cys20 - Cys40, Cys34 - Cys47; Lot No. P170320-MJ470307; MW = 5259.1 g/mol; Cat no.: 470307; Biomatik) and muscarine (Sigma-Aldrich) were dissolved in H_2O and stored at -20 degrees Celsius until required for experiments. A working concentration of 1 µM CART and 10 µM muscarine were used for in vitro experiments.

Assessment of recruitment properties

Recruitment properties of motor neurons subtypes were assessed during slow (100 pA/s) depolarizing current ramps which allowed us to measure the recruitment current and voltage threshold of the first action potential. The voltage threshold was defined when the change in voltage reached 10 mV/s. Firing rates were compared at three points on the frequency-current curve: at recruitment (minimum firing rate), 2 times recruitment current, and maximum firing rates.

Assessment of single action potential (spike) properties

Single spike properties (spike threshold, amplitude, rise time, half width) and AHP properties (amplitude and half width) were assessed with a 10 ms square pulse applied at an intensity 25% above rheobase. Spike threshold was determined as the potential at which the derivative (dV/dt) increased above 10 mV/s. Spike amplitude, rise time, and half width were measured from this point. AHP properties (amplitude and half width) were measured from baseline (-60 mV). Single spike and AHP properties were measured using event detection features in Clampfit.

Electrophysiology statistical analysis

Mixed-effects ANOVA were conducted to test the effect of pharmacological agents on intrinsic properties with a Geisser-Greenhouse's correction factor. Bonferroni post hoc analysis was performed when significant main effects were detected with a significance level of $p < 0.05$. Data are presented in figures as individual data points for all cells. Statistical analyses were performed using Graph Pad Version 9.0 (Prism, San Diego, CA, USA).

Hanging wire behavioral test and data analysis

The hanging wire test (reaches method) was used to assess muscle strength and coordination as was adapted from the Treat-NMD Neuromuscular Network standard operating protocol (Van Putten, 2011 DMD_M.2.1.004). Each mouse was handled by the experimenter for five consecutive days before the behavioral task. Mice were moved to the testing room 20-30 min prior to testing. All procedures and testing took place between 13:00-17:00 p.m. in an isolated testing room. A non-bending metallic wire (55cm long, 2.5mm thick) was attached to two transparent Plexiglas surfaces (40cm high) at a height approximately 35cm above soft bedding needed to break possible falls of the mouse. Each mouse handled by the tail by the experimenter was placed to the middle of the wire until it grasped it with all four limbs. For a period of 180sec the experimenter measured how many times the mouse would reach the one or the other end of the wire. Each time the mouse reached the end of the wire (1cm or less from the Plexiglas surface) the timer was stopped and the experimenter positioned the mouse at the middle of the wire hanging with all four limbs and facing the opposite Plexiglas surface. The timer would start again at this point. The number of reaches for each mouse during a three minutes period

was used for statistical analysis. Statistical analyses were performed using SPSS Version 22 (SPSS Inc, Chicago, IL, USA). The groups were compared using the independent samples t-test. Data from male and female mice were combined when there were no significant differences between them, or reported separately when they differed significantly. Four to six months old mice were used. Data are presented as mean values (±SEM). Statistical significance was set at $a < 0.05$ for all measures.

Supplementary Figures

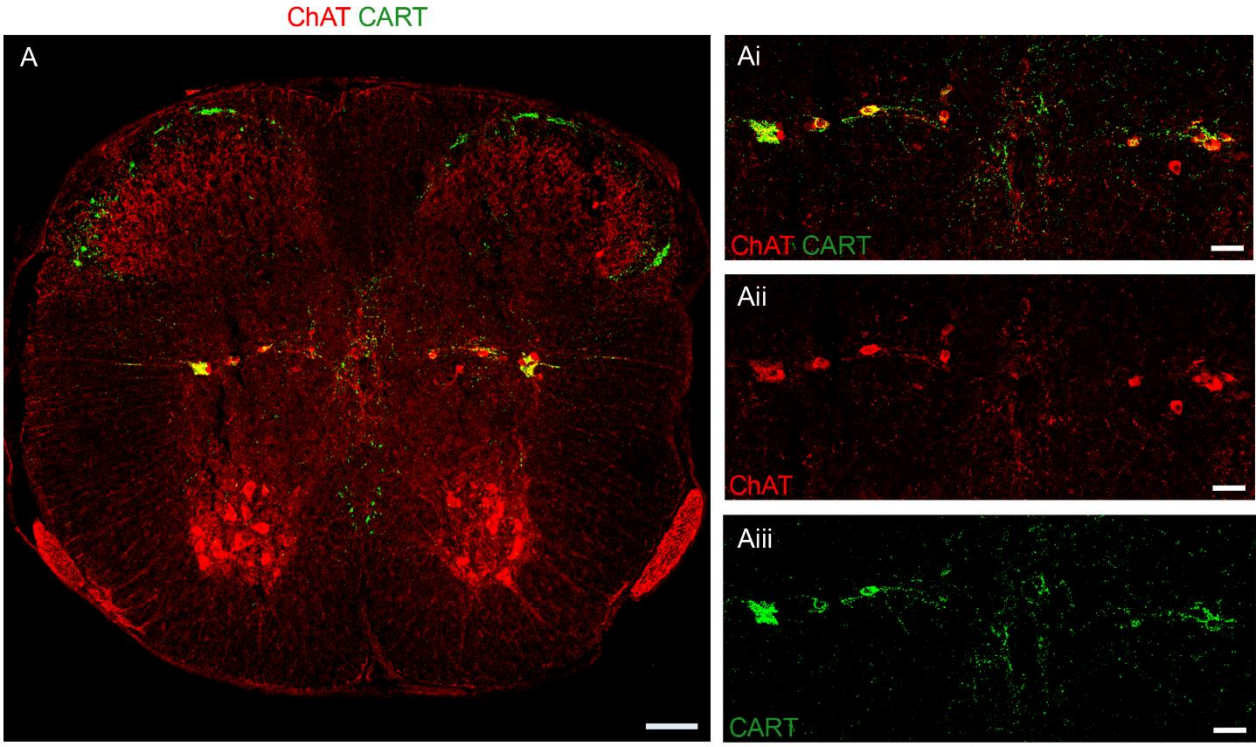

Fig. S1. Sympathetic preganglionic neurons express CART
(A) Immunofluorescence in thoracic spinal cord cross section of P25 mice with antibodies against CART (green) and ChAT (red). Sympathetic preganglionic cholinergic neurons express the CART peptide, reaffirming previous reports. (Ai-Aiii) Higher magnification panels focusing on the intermediate zone show merged and separate channels. Scale bars: (A) 100µm (Ai-Aiii) 20µm.

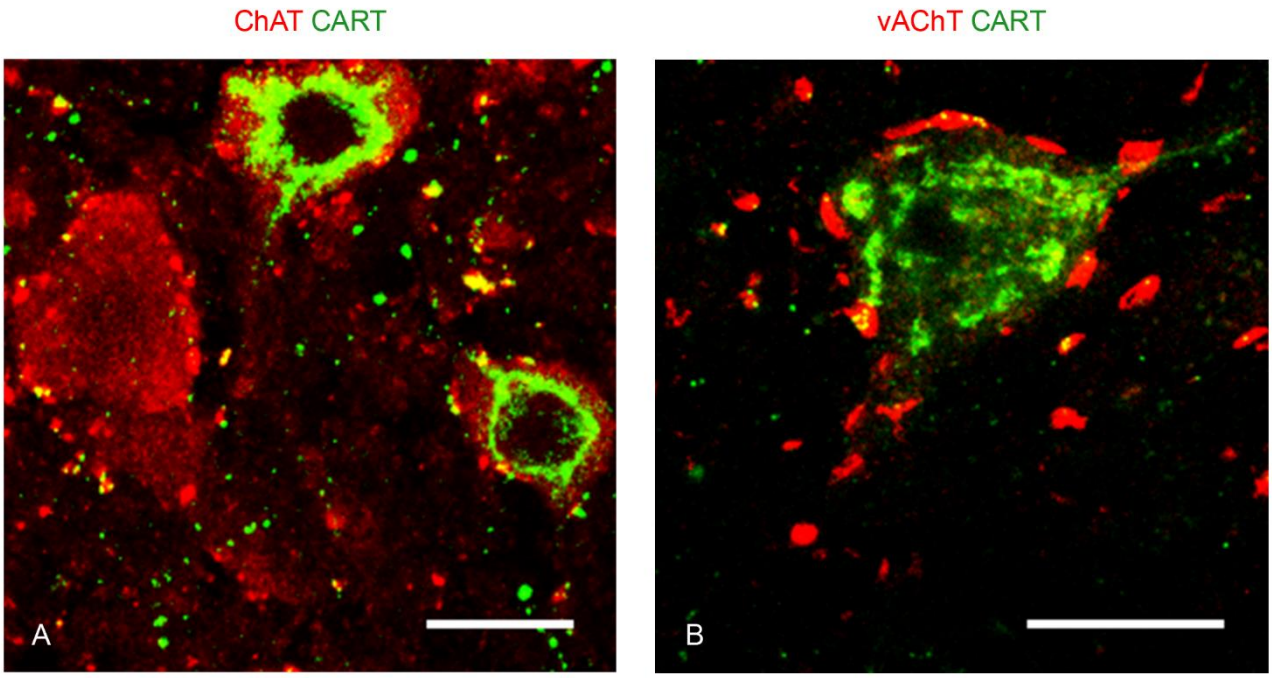

Fig. S2. A subset of motor neurons also expresses the CART neuropeptide
(A, B) Immunofluorescence for ChAT (red) and CART (green) reveals CART immunoreactivity in the somata of few motor neurons as well as CART+ C boutons on CART+ motor neurons. Scale bar: 20 µm

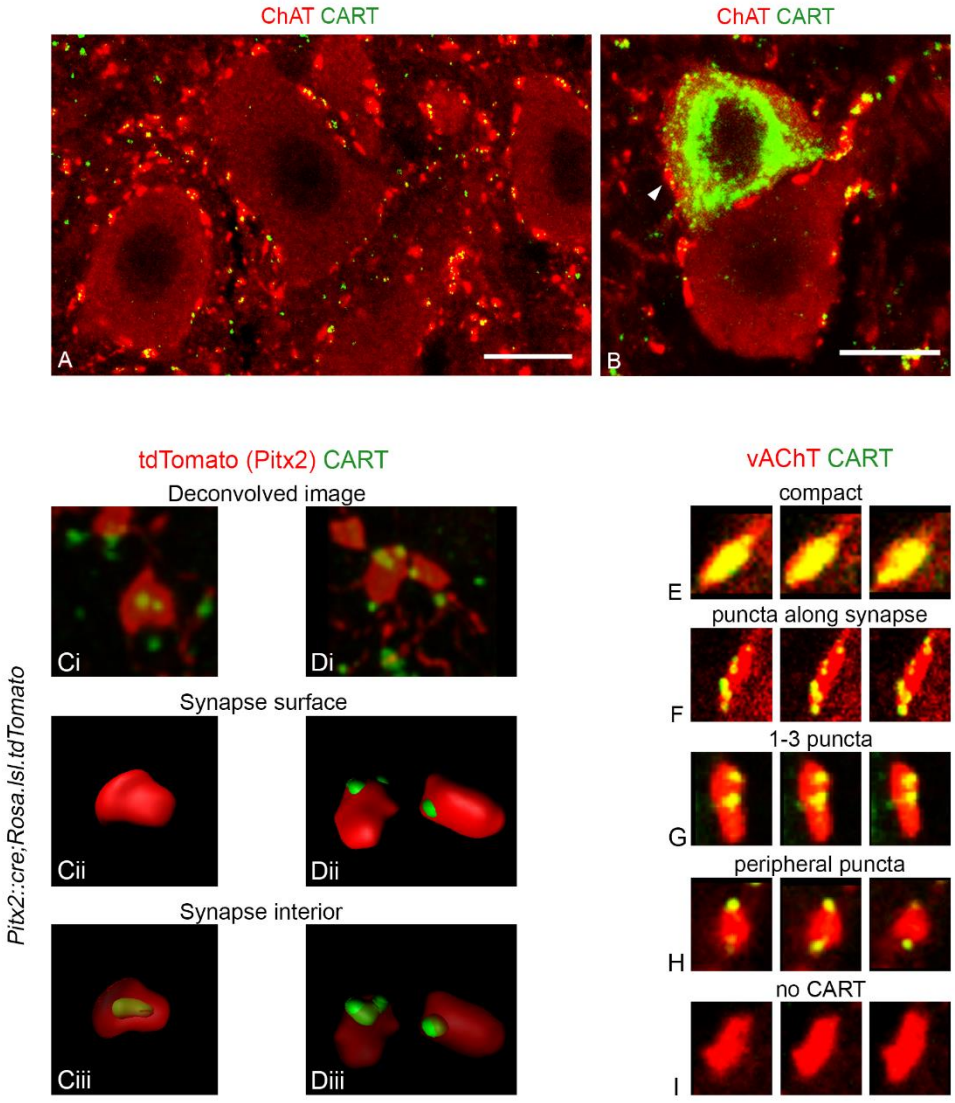

Fig. S3. Patterns of CART immunoreactivity in C boutons

(A) ChAT+ (red) C bouton synapses on the somata of motor neurons of P25 mice contain CART (green). Scale bar = 20 µm. (B) CART (green) is also present in few motor neuron somata. CART+ motor neurons also receive C bouton synapses that contain CART (white arrow); (P25). Scale bar=20 µm. (Ci-Ciii and Di-Diii) Immunofluorescence with antibodies against CART (green) and dsRed (red) label tdTomato+ C boutons in spinal cord cross sections of *Pitx2:Cre*;*Rosa.lsl.tdTomato* P25 mice. Single C bouton synapses were 3D reconstructed using the IMARIS software. (Ci and Di) High magnification (deconvolved) confocal images, used for the 3D reconstruction, showing the CART neuropeptide (green) within the synapse (red). (Cii and Dii) 3D reconstruction of the synapse surface (IMARIS). (Ciii and Diii) Rendering the synapse surface transparent reveals the distribution of CART inside the synapse. (E-I) The 5 different patterns of CART immunoreactivity in C boutons. E=compact, F=puncta along synapse, G=1-3 puncta, H=peripheral puncta, I= no CART.

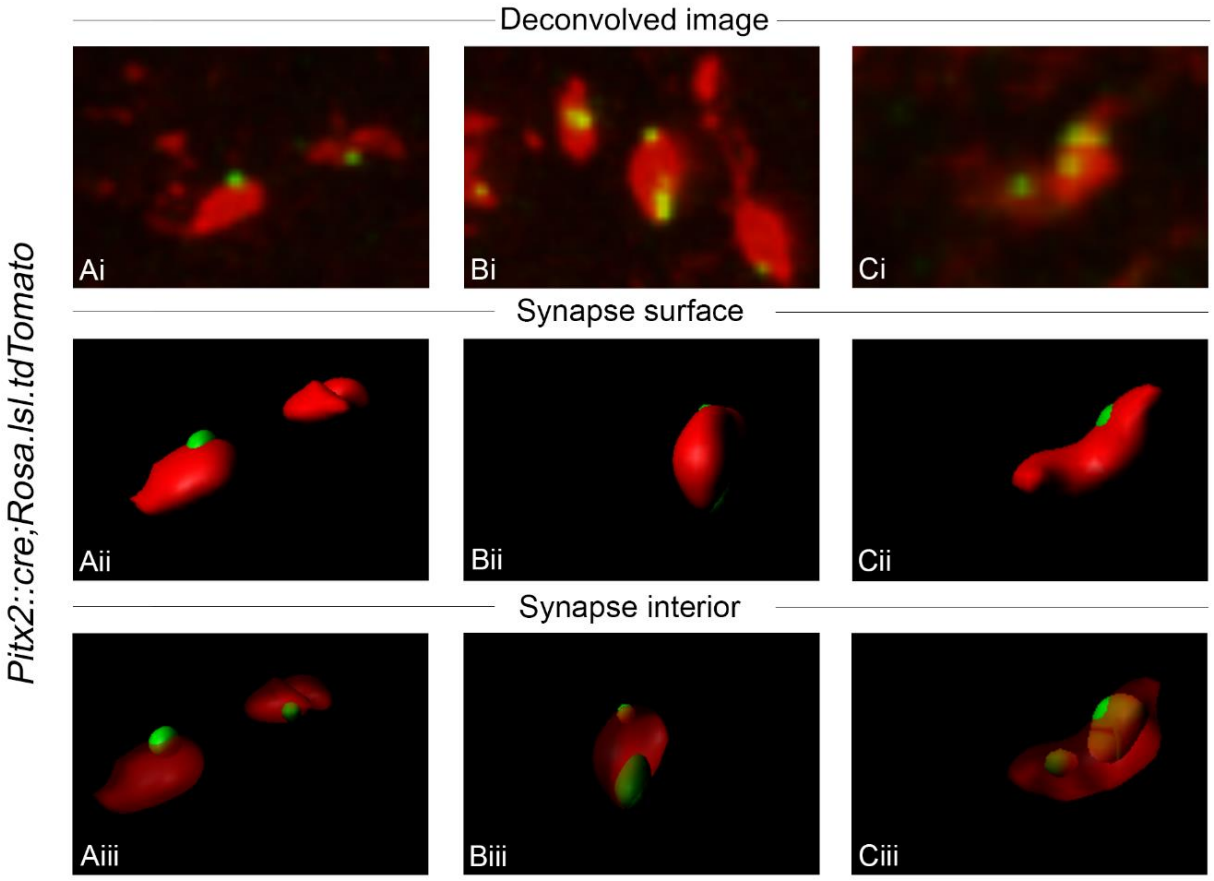

Fig. S4. 3D reconstruction of the C bouton synapse containing the CART neuropeptide IMARIS software-based 3D reconstruction of the synapse volume from confocal images of *Pitx2::Cre;Rosa.lsl.tdTomato* spinal cord sections with antibodies against dsRed (red) and CART (green). (Ai, Bi, Ci) Deconvolved z-stack images of the C bouton synapses used for the reconstruction. (Aii, Bii, Cii) The synapse volume is reconstructed in 3D. (Aiii, Biii, Ciii) The synapse is rendered transparent revealing the distribution of CART in the interior of the synapse.

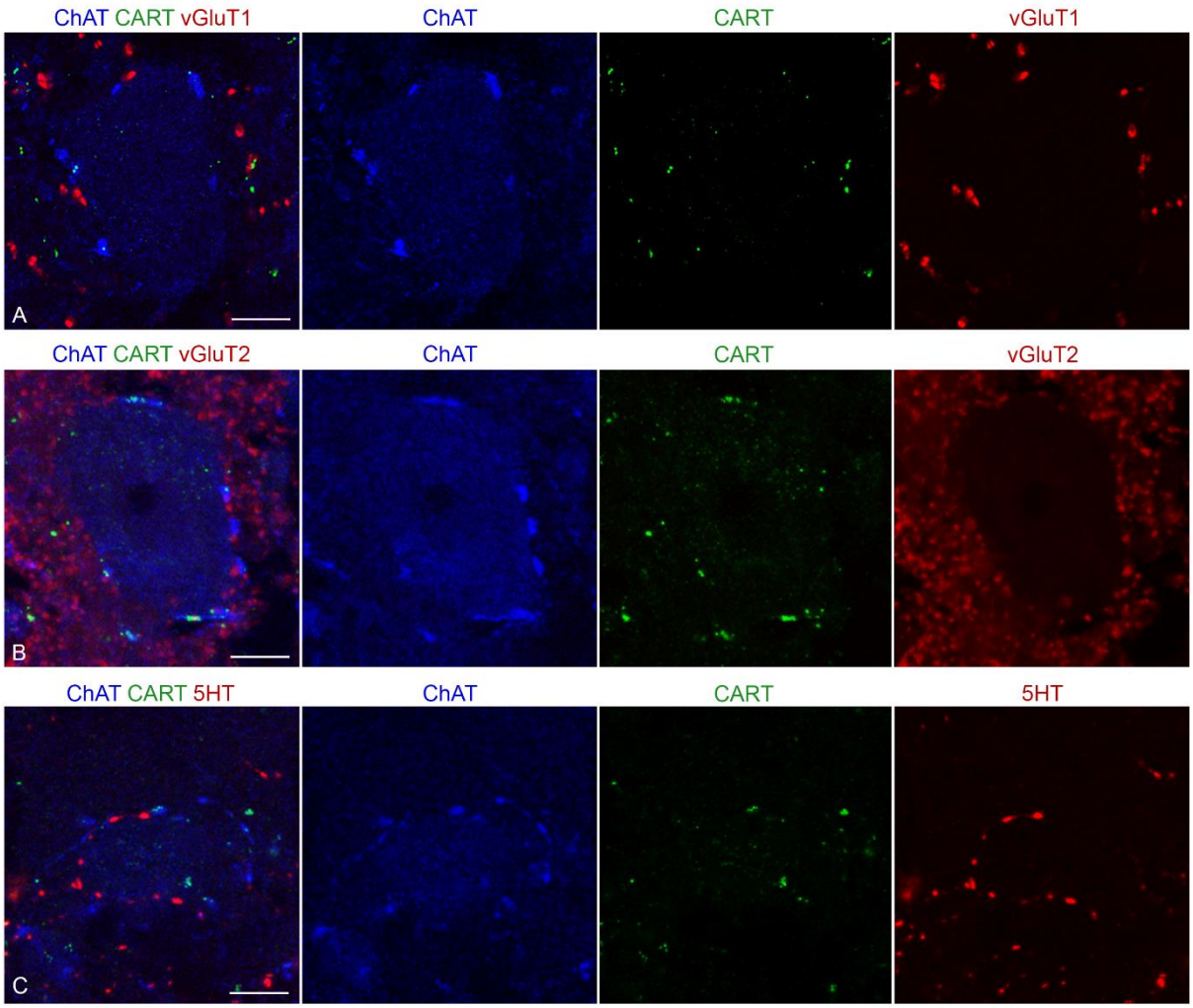

Fig. S5. CART is rarely colocalized in vGluT1, vGluT2 and 5HT synapses on motor neurons. (A) vGluT1+ (red) synapses detected on somata and proximal dendrites of motor neurons are not found to contain CART (green), except for a very low percentage, CART (green) is localized in ChAT+ (blue) C bouton synapses. (B) vGluT2+ (red) synapses are not found to contain CART (green), except for a very low percentage. (C) 5HT+ (red) synapses, rarely contain CART (green), in contrast with the ChAT+ (blue) C bouton synapses. Scale bars, 10μm.

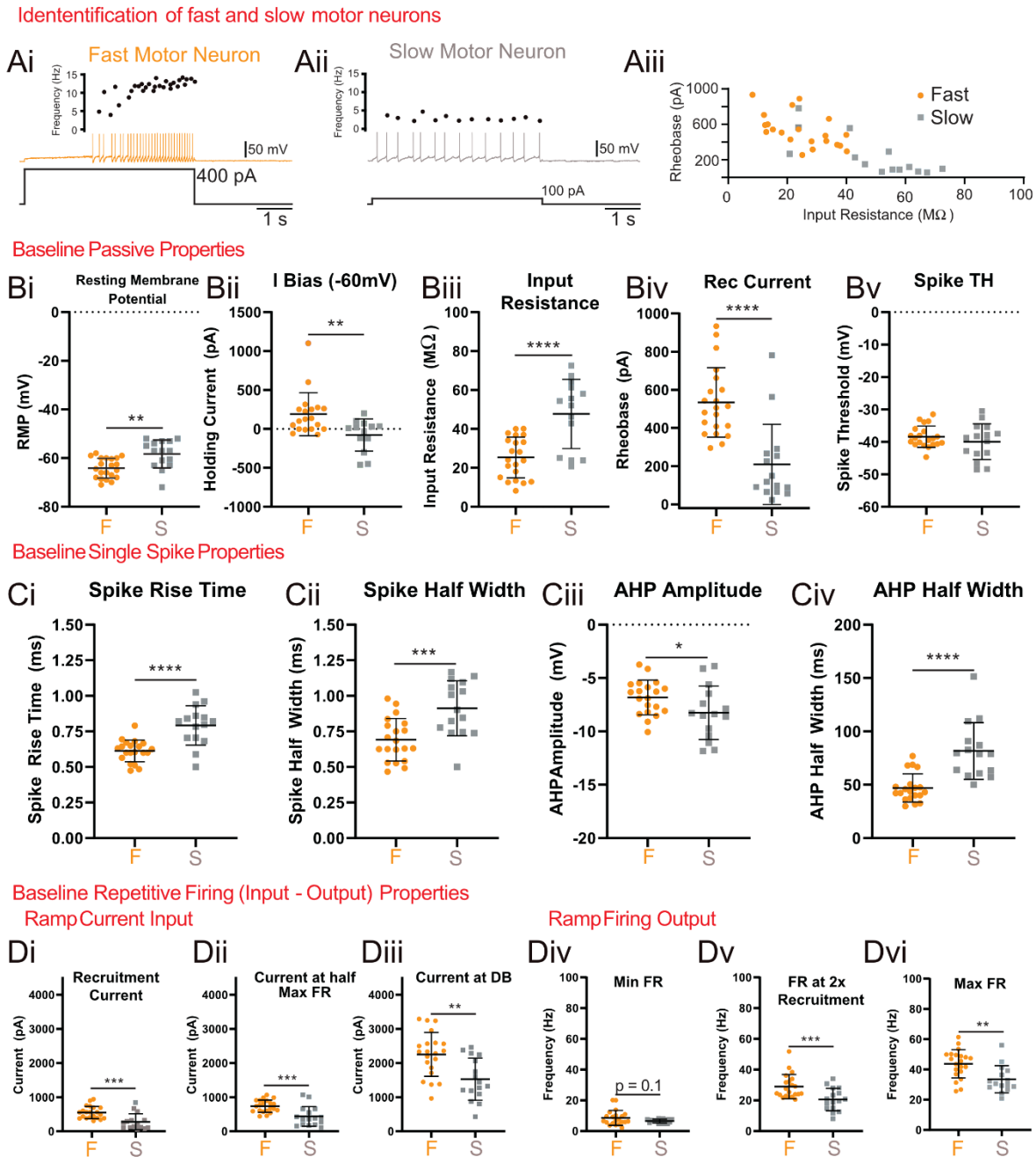

Fig. S6. Properties of fast and slow type motor neurons at baseline

(Ai-Aii) Representative traces of fast (Ai: Orange) and slow (Aii: grey) motor neurons identified with whole cell patch clamp electrophysiology which display delayed or immediate repetitive firing profiles, respectively. (Aiii) Scatter plot between input resistance and recruitment current (rheobase) demonstrate that fast motor neurons have a high rheobase, low input resistance, whereas slow motor neurons have a low rheobase and high input resistance. Compared to slow motor neurons, fast motor neurons have a significantly more hyperpolarized resting membrane potential (Bi), require more bias

current to bring the RMP to - 60 mV (Bii), have a lower input resistance (Biii), higher recruitment current (Biv), with no difference in spike threshold (Bv). Single action potential (spikes) features of fast motor neurons are significantly faster, with a shorter spike rise time (Ci) and half width (Cii). The medium afterhyperpolarization (mAHP) is significantly smaller in amplitude (Ciii) and shorter half width (Civ) in fast compared to slow motor neurons. The frequency-current (input-output) relationship was assessed on a slow depolarizing current ramp (100 pA/s). Input values (Currents) at repetitive firing onset (Di recruitment), half maximum firing (Dii) and depolarizing block (DB) (Diii) were significantly higher in fast compared to slow motor neurons. The output (firing rate) was not significantly different at recruitment (Div $p=0.1$) but was significantly higher in fast compared to slow motor neurons at 2x recruitment current (Dv) and maximal firing rates (Dvi). Horizontal black lines depict the mean and error bars represent standard deviation. Asterisks denote significance (*$p<0.05$, **$p<0.01$, ***$p<0.001$. ****$p<0.0001$) from unpaired t-test.

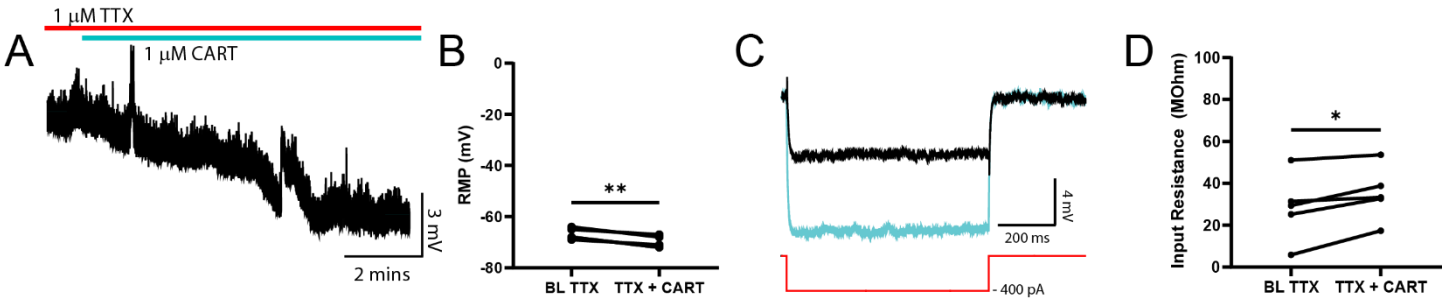

Fig. S7: CART hyperpolarizes the resting potential and increases input resistance of fast motor neurons in the presence of TTX.

(A) Representative trace of the resting membrane potential (RMP) of a fast motor neuron in the presence of tetrodotoxin (TTX: 1 µM, red bar) with subsequent application of CART (1 µM, blue bar). (B) CART hyperpolarizes the RMP in the presence of TTX. (C) Representative trace of the membrane potential in response to a hyperpolarizing current step before (black) and after application of CART (blue). (D) CART increases the input resistance in the presence of TTX. Data are displayed as individual data points from n = 5 fast motor neurons and analyzed using paired t-test. Asterisks denote significance (*p<0.05, **p<0.01).

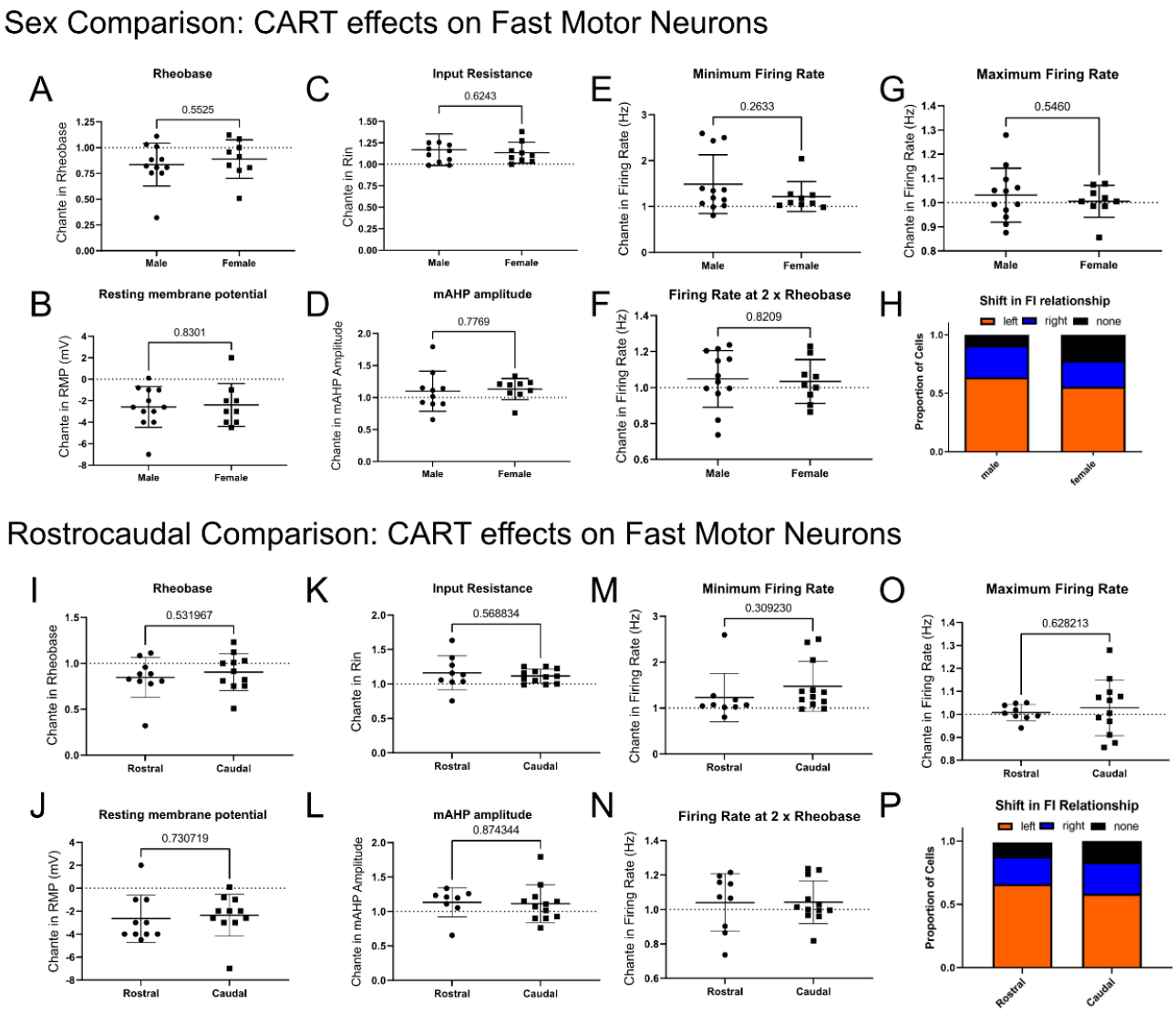

Fig. S8. The effects of CART on fast motor neurons are consistent between sexes and across lumbar spinal segments.

The magnitude of change produced by CART on fast motoneurons did not differ between sexes (male n = 12; female n = 9). Measurements made post-CART are normalized to their respective baselines to illustrate magnitude of change for Rheobase (A), Resting Membrane Potential (B), Input Resistance (C), Amplitude of the Medium Afterhyperpolarization (mAHP; D), Minimum Firing Rate on Ramp (E), Firing rate at 2 times Rheobase (F), and Maximum Firing Rate (G). There was no change in the proportion of cells that showed left, right, or no shift in their frequency-current relationships during slow depolarizing current ramps (H). Similar analyses were performed for the same parameters (I-P) measured from motor neurons in rostral (L1-L3) compared to caudal (L4-6) lumbar spinal segments (Rostral n = 10; Caudal n = 11). Data are displayed as individual data points with mean ± SD as lines superimposed over points. Data were analyzed using unpaired t-test, with p values displayed.

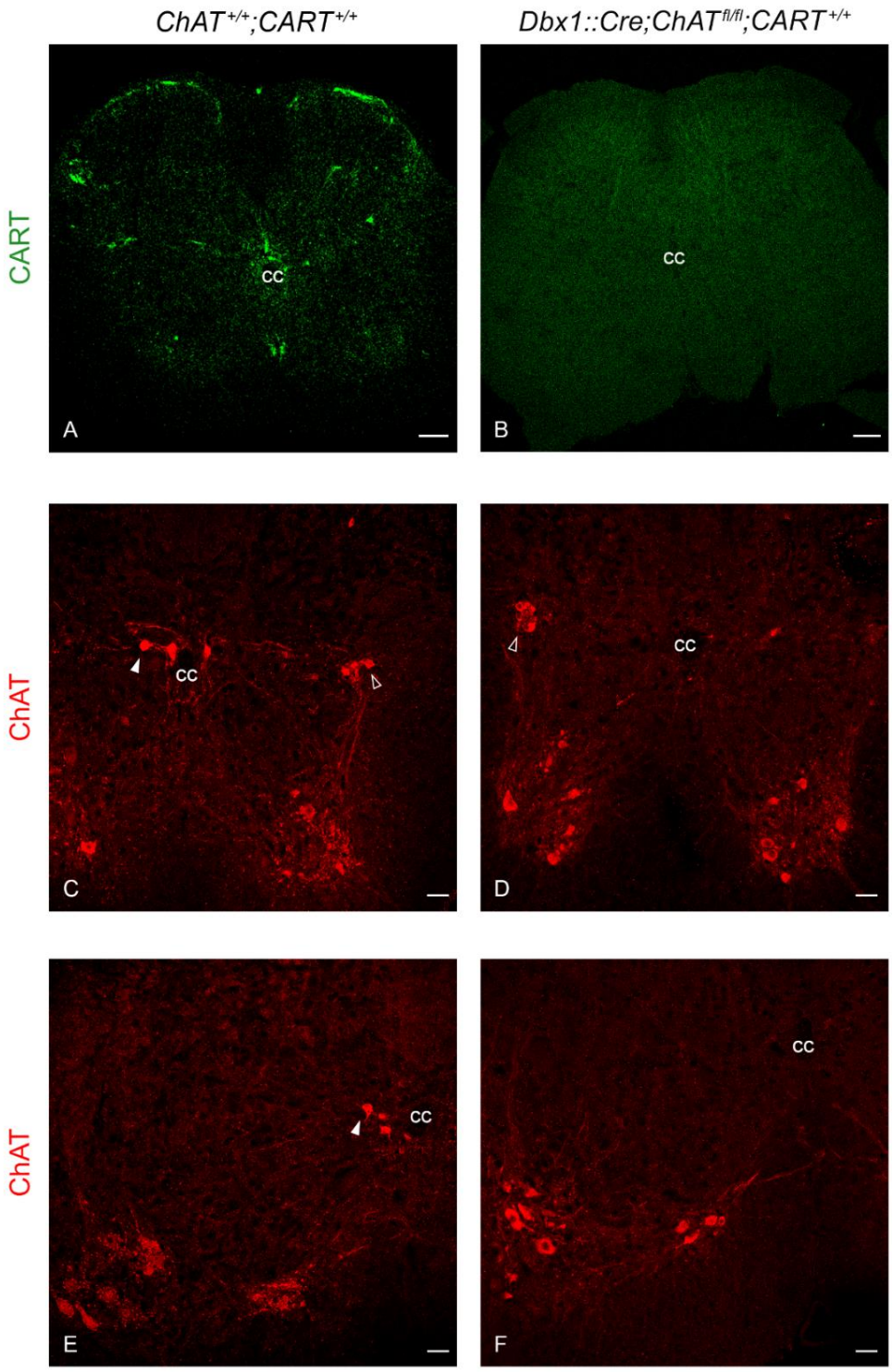

Fig. S9. Confirmation of the absence of CART peptide in *Cart* knockout mice and efficient removal of ChAT from V0c neurons

(A) Immunohistochemistry for the CART peptide in upper lumbar spinal cord cross section in wild type (*CART*$^{+/+}$;*ChAT*$^{+/+}$) mice, reveals strong signal. (B) Immunofluorescence for the CART peptide in upper lumbar spinal cord cross section of *Dbx1::Cre;ChAT*$^{fl/fl}$;*CART*$^{KO/KO}$ mice, reveals the complete absence of fluorescent signal, confirming the total KO of the Cartpt gene. (C) Immunohistrochemistry for ChAT in thoracic spinal cord cross section of wild type (*CART*$^{+/+}$;*ChAT*$^{+/+}$) mice, reveals ChAT+ Dbx1 derived V0c interneurons (white solid arrowhead) as well as ChAT+ SPNs (empty arrowhead). (D) In

Dbx1::Cre;ChAT$^{fl/fl}$;CART$^{KO/KO}$ mice the Dbx1 derived V0c cholinergic interneurons are no longer ChAT+ while SPNs are still ChAT+ (empty arrowhead), proving the successful conditional KO of the ChAT gene specifically in V0c interneurons. (E) In mid lumbar sections of wild type (*CART$^{+/+}$;ChAT$^{+/+}$*) mice SPNs are not present, therefore only ChAT+ Dbx1 derived V0c interneurons are detected (white solid arrowhead). (F) In *Dbx1::Cre;ChAT$^{fl/fl}$;CART$^{KO/KO}$* mice a complete absence of ChAT+ signal in the cc region reveals the successful conditional KO of the ChAT gene from V0c interneurons. cc: cental canal. Scale bars: 50µm

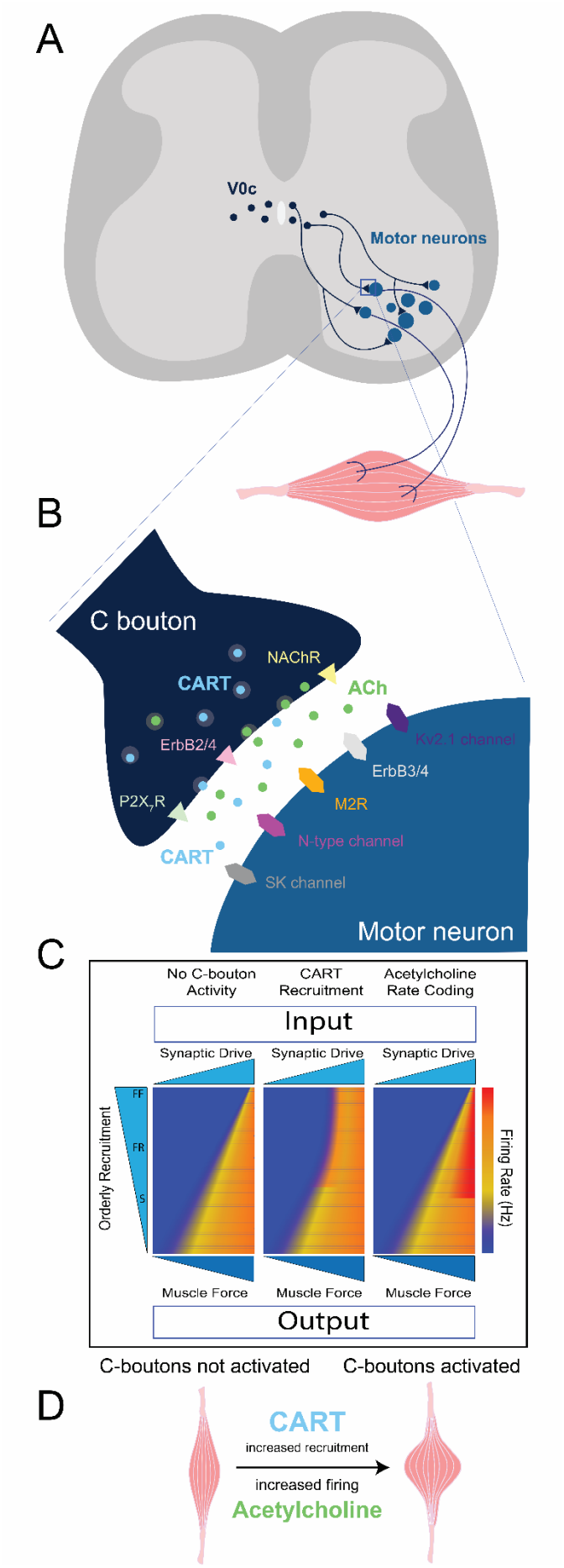

Fig. S10. Proposed model of the effect of C bouton function in motor neuron output through acetylcholine and CART signaling

(A) Schematic representation of a spinal cord cross section. Dark blue dots represent the V0c somata in the vicinity of the central canal, the axons of which innervate fast and slow motor neuron somata (light blue) in lamina IX (only axons travelling on the same level shown for simplicity). The framed area indicates a single C bouton synapse magnified in B. (B) Schematic representation of a single C bouton. The presynaptic terminal (dark blue) contains vesicles loaded with acetylcholine (green) as well as what we propose are Dense Core Vesicles (DCVs) containing the CART peptide (light blue). The presynaptic ATP receptors P2X7R (light green triangles) the ErbB2/4 NRG1 receptors (light pink triangles) and the NAChR - Nicotinic Acetylcholine receptors (light yellow triangles) are also depicted. In the postsynaptic terminal (light blue) SK Ca2+ dependent K+ channels (grey), N-type voltage dependent K+ channels (magenta) and ErbB3/4 NRG1 receptors (light grey) as well as Kv2.1 K+ channels (purple) and M2-muscarinic type 2 acetylcholine receptors- (orange), are presented. (C) Schematic representation of how orderly recruitment of slow (S), fast fatigue resistant (FR), and fast fatigable (FF) motor neuron subtypes, and their respective firing rate (heat map) transform synaptic drive (input) to muscle force (output). CART increases output by decreasing the recruitment threshold of fast motor neurons, acetylcholine increases output by increasing fast motor neuron maximal firing rate. (D) Suggested effect of C bouton activation in muscle contraction. The combinatorial effect of the CART peptide increasing motor neurons recruitment and acetylcholine increasing the motor neurons' firing rate leads to a pronounced muscle contraction.

Table S1. Effects of CART or Muscarine on the intrinsic properties of fast motor neurons. The number of motor neurons studied, and animals used for each condition are included in parentheses in row 1 (MNs, animals). Data are presented as mean±SD (min, max). Statistics: data were analyzed using a repeated-measures ANOVA. F and p values are reported for each statistical test. Asterisks denote significance from Holm-Sidak post hoc comparisons, * p<0.05, ** p<0.01. *** p<0.001, **** p<0.0001. Red text signifies a significant decrease and green text a significant increase.

Fast Motor Neurons			
Parameter		**1 µM CART (n_{MN}=21, n_{mice}=11)**	**10 µM Muscarine (n_{MN} =12, n_{mice}=6)**
Resting membrane potential (mV)			
	Baseline	-64.1±4.1 (-71,-58)	-63.2±4.0(-67,-48)
	Drug	-66.6±4.1(-72,-59)****	-59.3±6.1(-67,-48)**
	Wash	-66.4±4.3(-72,-60)**	-64.8±3.2(-68,-58)
	ANOVA (F,p)	19.6, 0.00002	14.0,0.0005
Input resistance (MΩ)			
	Baseline	25.3±10.5(8.2,40.1)	23.0±10.8(8.5,45.3)
	Drug	27.6±10.1(13.4,50.0)*	23.8±11.3(7.5,42.5)
	Wash	29.7±14.2(11.6,62.2)**	24.0±9.0(12.4,35.5)
	ANOVA (F,p)	7.6, 0.003	6.1,0.02
Recruitment current on ramp (pA)			
	Baseline	534±182(295,933)	491±233(205,868)
	Drug	452±144(175,727)*	493±286(170,1216)
	Wash	515±201(175,911)	660±399(212,1290)
	ANOVA (F,p)	3.5,0.05	3.9,0.12
First spike threshold on ramp (mV)			
	Baseline	-38.4±3.3(-44.7,-31.5)	-39.5±2.4(-42.9,-34.9)
	Drug	-38.9±4.2(-44.9,-32.2)	-41.3±2.7(-46.7,-38.2)
	Wash	-38.3±3.9(-45.4,-33.0)	-39.8,2.9(-44.6,-36.3)
	ANOVA (F,p)	0.3,0.7	5.4,0.08
Action potential rise time (ms)			
	Baseline	0.61±0.08(0.47,0.79)	0.56±0.14(0.2,0.75)
	Drug	0.64±0.03(0.47,0.99)	0.62±0.1(0.43,0.83)
	Wash	0.65±0.1(0.48,0.80)	0.62±0.1(0.45,0.80)
	ANOVA (F,p)	1.7,0.2	2.9,0.13
Action potential half width (ms)			
	Baseline	0.69±0.15(0.47,0.98)	0.60±0.1(0.46,0.76)
	Drug	0.70±0.14(0.49,0.93)	0.65±0.1(0.47,0.78)
	Wash	0.71±0.16(0.49,0.96)	0.62±0.06(0.54,0.69)
	ANOVA (F,p)	3.2,0.08	5.2,0.02
Afterhyperpolarization amplitude (mV)			
	Baseline	6.7±1.6(3.7,10.1,)	6.8±2.1(3.9,9.4)
	Drug	7.7±2.2(4.3,12.1,)**	3.5±2.0(1.1,8.1)****
	Wash	8.2±2.4(4.0,12.9)***	6.2±2.9(1.7,10.1)
	ANOVA (F,p)	12.1, 0.001	19.7,0.0002
Afterhyperpolarization half width (ms)			
	Baseline	46.9±13.6(29.8,76.8)	37.2±12.3(20.6,59.9)
	Drug	49.3±14.9(33.4,82.2)*	31.0±3.5(9.8,52.3)
	Wash	49.4±14.9(32.0,83.5)	33.2±13.8(16.8,61.3)
	ANOVA (F,p)	5.3,0.02	5.1,0.07
Minimum firing rate (Hz)			
	Baseline	7.7±4.1(2.1,20.1)	8.2±3.4(4.6,14.1)
	Drug	9.9±4.2(4.6,21.5)**	10.3±5.9(3.5,26.5)
	Wash	8.1±3.5(1.9,14.7)	8.6±5.9(3.5,18.6)
	ANOVA (F,p)	6.6,0.004	1.8,0.2
Firing rate at 2x recruitment current (Hz)			
	Baseline	27.8±7.5(20.6,51.8)	29.9±10.6(16.2,55.9)
	Drug	29.7±8.8(19.5,55.6)*	42.9±13.3(26.0,66.7)**
	Wash	29.5±6.7(20.6,45.4)	38.3±16.9(10.1,64.5)
	ANOVA (F,p)	3.4,0.03	9.2,0.006
Maximum Firing Rate (Hz)			
	Baseline	43.5±9.7(25.6,61.3)	48.9±13.0(34.0,83.3)
	Drug	44.3±9.9(23.3,62.5)	58.6±16.0(38.2,95.2)*
	Wash	42.9±8.5(25.3,55.6)	56.6±14.4(37.2,84.8)
	ANOVA (F,p)	1.2,0.3	7.6,0.03

Table S2. Effects of CART or Muscarine on the intrinsic properties of slow motor neurons. The number of motor neurons studied, and animals used for each condition are included in parentheses in row 1 (MNs, animals). Data are presented as mean±SD (min, max). Statistics: data were analyzed using a repeated-measures ANOVA. F and p values are reported for each statistical test. Asterisks denote significance from Holm-Sidak post hoc comparisons, * p<0.05, ** p<0.01. *** p<0.001, **** p<0.0001.

Slow Motor Neurons			
Parameter		**1 µM CART (n_{MN}=15, n_{mice}=6)**	**10 µM Muscarine (n_{MN}=7, n_{mice}=4)**
Resting membrane potential (mV)			
	Baseline	-58.6±5.7 (-72,-52)	-58.6±7.2 (-67,-48)
	Drug	-59.6±6.6 (-72,-46)	-57.3±6.8 (-67,-48)
	Wash	-60.4±5.6 (-72,-52)	-61.4±7.9 (-68,-48)
	ANOVA (F,p)	0.9, 0.4	5.1, 0.1
Input resistance (MΩ)			
	Baseline	230±221 (23,781)	54±39 (25,129)
	Drug	273±21 (30,671)	50±41 (21,141)
	Wash	246±242 (28,710)	63±56 (22,160)
	ANOVA (F,p)	1.0, 0.07	2.0, 0.2
Recruitment current on ramp (pA)			
	Baseline	64.7±71.6 (20.8,326.0)	197±190 (55,525)
	Drug	60.9±61.7 (15.5,283.0)	238±232 (86,676)
	Wash	66.0±62.2 (17.7,263.0)	243±265 (94,714)
	ANOVA (F,p)	0.6, 0.4	3.1, 0.2
First spike threshold on ramp (mV)			
	Baseline	-39.5±5.6(-48.5,-30.5)	-40.2±1.9 (-43.2,-37.6)
	Drug	-38.9±6.2(-49.0,-27.1)	-38.8±2.5 (-41.7,-34.5)
	Wash	-39.8±5.6(-48.3,-30.2)	-40.5±2.7 (-44.1,-37.2)
	ANOVA (F,p)	0.3,0.7	6.5,0.2
Action potential rise time (ms)			
	Baseline	0.79±0.14 (0.50,1.02)	0.67±0.18 (0.50,0.92)
	Drug	0.80±0.15 (0.44,1.06)	0.65±0.14 (0.47,0.94)
	Wash	0.84±0.16 (0.64,1.14)	0.68±0.12 (0.51,0.80)
	ANOVA (F,p)	0.7, 0.5	0.4, 0.6
Action potential half width (ms)			
	Baseline	0.91±0.2 (0.50,1.16)	0.71±0.12 (0.53,0.86)
	Drug	0.94±0.2 (0.59,1.26)	0.68±0.16 (0.47,0.93)
	Wash	0.98±0.2 (0.71,1.42)	0.66±0.14 (0.48,0.86)
	ANOVA (F,p)	2.7, 0.13	0.6, 0.5
Afterhyperpolarization amplitude (mV)			
	Baseline	8.3±2.5 (3.9,11.8)	7.1±2.7 (3.4,11.6)
	Drug	8.5±3.4 (3.8,13.9)	4.2±2.2 (1.3,7.8)
	Wash	9.5±3.1 (5.4,14.8)	5.3±3.5 (1.1,9.0)
	ANOVA (F,p)	0.7, 0.5	4.8, 0.08
Afterhyperpolarization half width (ms)			
	Baseline	81.7±26.6 (50.1,151.5)	69.5±27.3 (37.6,109.6)
	Drug	84.3±27.5 (49.1(143.6)	42.1±15.8 (13.3,61.9)
	Wash	89.3±31.5 (54.3,156.8)	44.5±25.0 (11.6,79.9)
	ANOVA (F,p)	2.4, 0.07	4.9, 0.05
Minimum firing rate (Hz)			
	Baseline	6.4±1.3 (4.6,8.3)	4.2±1.7 (1.5,6.6)
	Drug	5.6±1.5 (2.4,8.4)	5.5±1.9 (3.3,8.8)
	Wash	5.9±1.3 (4.1,7.6)	5.7±2.2 (4.0,8.9)
	ANOVA (F,p)	1.8, 0.2	4.5, 0.2
Firing rate at 2x recruitment current (Hz)			
	Baseline	19.6±6.6 (8.0,30.8)	21.1±11.3 (9.8,40.8)
	Drug	19.8±7.4 (8.5,14.4)	24.6±14.2 (12.0,48.8)
	Wash	20.6±7.5 (8.7,30.6)	21.4±15.5 (11.1,44.3)
	ANOVA (F,p)	1.8, 0.09	1.2, 0.3
Maximum Firing Rate (Hz)			
	Baseline	33.5±9.0 (20.9,56.0)	48.2±6.9 (40.7,60.2)
	Drug	31.8±9.4 (16.0,52.4)	51.3±9.8 (37.2,60.6)
	Wash	33.3±8.2 (17.8,50.8)	48.0±9.3 (36.2,58.8)
	ANOVA (F,p)	0.5, 0.5	0.8, 0.4

Table S3. Comparison of the number of vAChT+ terminals, M2 receptor clusters and instances of their alignment between control and *Dbx1::Cre; ChAT$^{fl/fl}$; CART$^{KO/KO}$* mice.

vAChT + terminals number evaluation											
mice (N)		**motor neurons (n)**		**MWU**	**P value**	**median**		**mean**		**SE mean**	
ctrl	exp	ctrl	exp			ctrl	exp	ctrl	exp	ctrl	exp
3	4	61	64	1867	0.6730	6.000	6.000	6.891	6.639	0.2929	0.3022
M2 receptor clusters number evaluation											
ctrl	exp	ctrl	exp			ctrl	exp	ctrl	exp	ctrl	exp
3	4	45	49	1001	0.4402	7.000	7.000	7.178	6.775	0.3586	0.3395
vAChT-M2 alignment instances number evaluation											
ctrl	exp	ctrl	exp			ctrl	exp	ctrl	exp	ctrl	exp
3	4	45	49	963	0.2880	7.00	6.000	7.022	6.490	0.3644	0.3415

Table S4. Comparison of the size of of vAChT+ terminals and M2 receptor clusters between control and *Dbx1::Cre; ChAT$^{fl/fl}$; CART$^{KO/KO}$ mice*.

vAChT + terminals size evaluation											
mice (N)		**synapses (n)**		**MWU**	**P value**	**median**		**mean**		**SE mean**	
ctrl	exp	ctrl	exp			ctrl	exp	ctrl	exp	ctrl	exp
3	3	250	228	25733	0.0666	2.060	1.950	2.104	2.010	0.04124	0.04322
M2 receptor clusters size evaluation											
ctrl	exp	ctrl	exp			ctrl	exp	ctrl	exp	ctrl	exp
3	3	225	254	25658	0.0537	2.030	2.160	2.110	2.217	0.04238	0.03988

Supplementary References

1. L. Zagoraiou, *et al.*, A cluster of cholinergic premotor interneurons modulates mouse locomotor activity. *Neuron* **64**, 645–662 (2009).

2. N. Schaeren-Wiemers, A. Gerfin-Moser, A single protocol to detect transcripts of various types and expression levels in neural tissue and cultured cells: in situ hybridization using digoxigenin-labelled cRNA probes. *Histochemistry* **100**, 431–440 (1993).

3. W. Liu, J. Selever, M. F. Lu, J. F. Martin, Genetic dissection of Pitx2 in craniofacial development uncovers new functions in branchial arch morphogenes, late aspects of tooth morphogenesis and cell migration. *Development* **130**, 6375–6385 (2003).

4. L. Madisen, *et al.*, A robust and high-throughput Cre reporting and characterization system for the whole mouse brain. *Nature Neuroscience 2009 13:1* **13**, 133–140 (2009).

5. F. Bielle, *et al.*, Multiple origins of Cajal-Retzius cells at the borders of the developing pallium. *Nat Neurosci* **8**, 1002–1012 (2005).

6. M. Buffelli, *et al.*, Genetic evidence that relative synaptic efficacy biases the outcome of synaptic competition. *Nature* **424**, 430–434 (2003).

7. T. Misgeld, *et al.*, Roles of neurotransmitter in synapse formation: Development of neuromuscular junctions lacking choline acetyltransferase. *Neuron* **36**, 635–648 (2002).

8. N. Wierup, *et al.*, CART knock out mice have impaired insulin secretion and glucose intolerance, altered beta cell morphology and increased body weight. *Regul Pept* **129**, 203–211 (2005).

9. J. Schindelin, *et al.*, Fiji: an open-source platform for biological-image analysis. *Nature Methods 2012 9:7* **9**, 676–682 (2012).

10. F. Leroy, B. Lamotte d'Incamps, R. D. Imhoff-Manuel, D. Zytnicki, Early intrinsic hyperexcitability does not contribute to motoneuron degeneration in amyotrophic lateral sclerosis. *Elife* **3** (2014).

11. F. Leroy, B. L. d'Incamps, D. Zytnicki, Potassium currents dynamically set the recruitment and firing properties of F-type motoneurons in neonatal mice. *J Neurophysiol* **114**, 1963–1973 (2015).

12. S. A. Sharples, G. B. Miles, Maturation of persistent and hyperpolarization-activated inward currents shapes the differential activation of motoneuron subtypes during postnatal development. *Elife* **10** (2021).